



# Characterization of road dust and resuspended particles close to a busy road of Venice mainland (Italy)

G. Valotto<sup>1</sup> · D. Zannoni<sup>1,2</sup> · P. Guerriero<sup>2</sup> · G. Rampazzo<sup>1</sup> · F. Visin<sup>1</sup>

Received: 29 August 2018 / Revised: 21 January 2019 / Accepted: 28 January 2019 / Published online: 4 February 2019  
© Islamic Azad University (IAU) 2019

## Abstract

Road traffic contributes to atmospheric particulate matter with exhaust (fuel combustion) and non-exhaust (wear of vehicle parts such as brake, tires and abrasion of the road surface) emissions. Road dust is composed of particles belonging to natural and anthropogenic sources related in large part to road traffic. To date, understanding the relative contribution of road dust resuspension and particles directly emitted by abrasion to particulate matter is still a matter of debate. In this work, road dust and resuspended particles samples are collected at different heights and with increasing sampling time near a busy road of Venice mainland. Elemental composition and morphology of particles were investigated with a combination of techniques: inductively coupled plasma optical emission spectroscopy (ICP-OES), inductively coupled plasma mass spectrometry (ICP-MS), laser diffraction analysis and scanning electron microscopy–energy-dispersive X-ray spectrometry (SEM–EDX). The differences between deposited and resuspended particles were highlighted and the main pollutant sources were identified to study the resuspension process related to the traffic flow. Resuspended particles were divided into six groups related to the presence of anti-ice material, to soil resuspension and to the road surface and vehicle parts wear. The contributions of clustered particles vary with the height from the road level. This study, the first one focusing on the road traffic particles resuspension in Veneto region, will provide topical information for the identification of this source in atmospheric particulate samples.

**Keywords** Road dust · Particle resuspension · Particle identification · Road traffic · SEM/EDX

## Introduction

Road traffic is an important source of atmospheric particulate in urban and industrial environments, especially close to busy roads, street canyons and inside tunnels (Kumar et al.

2013; Pant and Harrison 2013; Amato et al. 2014; Grigoratos and Martini 2015; Timmers and Achten 2016). The contribution of road traffic to particulate matter includes exhaust and non-exhaust emissions. Exhaust emissions are related to fuel combustion, while non-exhaust emissions originate from brake systems (pads and disks), tires and road surface wear and also to road dust (RD) resuspension (Valotto et al. 2015).

Up to now, policy actions and technological upgrades in the car industry were mainly aimed to reduce the impact of exhaust emissions on atmospheric particulate matter. This fact has implicated an increase in the percentage contribution of non-exhaust sources to particulate matter (Bukowiecki et al. 2009; Rexeis and Hausberger 2009; Timmers and Achten 2016). It was estimated that approximately 60% of the total traffic-related PM<sub>10</sub> emissions are due to non-exhaust emissions and to resuspension of RD (Bukowiecki et al. 2009). The relative contribution of non-exhaust sources to the total emission of road traffic is expected to increase up to 90% in the future (Rexeis and Hausberger 2009). The

---

Editorial responsibility: Mohamed F. Yassin.

---

**Electronic supplementary material** The online version of this article (<https://doi.org/10.1007/s13762-019-02246-1>) contains supplementary material, which is available to authorized users.

---

✉ D. Zannoni  
daniele.zannoni@unive.it

<sup>1</sup> Department of Environmental Sciences, Informatics and Statistics, Ca' Foscari University of Venice, Via delle Industrie n. 21/8 c/o INCA-VEGAPARK, 30175 Marghera, VE, Italy

<sup>2</sup> Institute of Condensed Matter Chemistry and Technologies for Energy, National Research Council of Italy ICMATE-CNR, Corso Stati Uniti, 4, 35127 Padua, Italy



growing spread of hybrid and electric cars will significantly increase the percentage contribution of non-exhaust sources in this regard. Such types of vehicles are characterized by relatively high weight which promotes higher brakes, tires and asphalt wear. Indeed, on average an electric vehicle is 24% heavier than the equivalent internal combustion engine (Timmers and Achten 2016).

Particles sourced to non-exhaust emission are potential carriers of harmful compounds and heavy metals (Pant and Harrison 2013; Shi et al. 2011). However, up to now a dedicated and recognized model to perform the risk assessment for these sources does not exist. For example, most of the works focusing on the exposure pathways of RD matrix and the respective potential health risks (Wan et al. 2016; Valotto et al. 2018) use the approaches provided by US Environmental Protection Agency for estimating soil contamination (USEPA 1996). Moreover, although the contribution of RD resuspension prevails in some European areas (Amato et al. 2014; Karanasiou et al. 2014), the technical guidance of European Environment Agency (EMEP/EEA 2016) for the evaluation of non-exhaust contributions does not include resuspension. Otherwise, more complex models such as TNO URBIS (Amato et al. 2016) and NORTRIP (Denby et al. 2013) consider also the RD resuspension to predict the whole non-exhaust particle emissions.

The chemical composition of RD, its size distribution and the respective percentage contribution to the atmospheric particulate by resuspension depend site by site. Indeed, these features are related to the following key aspects: traffic flow, fleet composition, vehicles tires and brake composition, roads type, climate conditions as well as geology of the sampling site (Bukowiecki et al. 2009; EMEP/EEA 2016; Pant and Harrison 2013; Valotto et al. 2018). It is worth noting that discriminating between particles related to resuspension and those directly emitted from vehicle parts abrasion is still an open issue and this research field is gaining much more attention in the last few years (Grigoratos and Martini 2015).

Venice Municipality is located in northern Italy, in the eastern part of the Po Plain bordered by the Adriatic Sea. This area is one of the largest industrial areas in Italy and is affected by different types of atmospheric particulate matter emission sources. These sources are related to activities in the Mestre and Venezia urban areas, in the industrial setting of Porto Marghera including marine, air and heavy/light road traffic (Valotto et al. 2014). According to INEMAR (INventario EMissioni Regione Veneto (INEMAR) 2006) which is the emission inventory of Veneto Region, the fuel combustion related to the macrosector “road transport” was the third source of atmospheric particulate in Venice Municipality in 2013.

In this work, RD and resuspended particles samples were collected at different heights and with increasing sampling times from the road level near a busy highway of Venice Mainland (Italy) between December 2016 and January 2017. The chemical composition and the morphology of particles were determined using a combination of technique in order to study the resuspension process related to the traffic flow, highlighting the differences between deposited and resuspended particles and identifying the main pollutant sources.

Inductively coupled plasma optical emission spectroscopy (ICP-OES), inductively coupled plasma mass spectrometry (ICP-MS) and laser diffraction analysis were used to determine the elemental composition and the particles size distribution of RD samples. Scanning electron microscopy coupled with energy-dispersive X-ray spectrometry (SEM-EDX) was used to study the elemental composition and the morphological aspects of resuspended particles. Furthermore, the relations between elemental concentrations and morphology values were studied by cluster analysis.

This study is intended to provide important information for the identification of RD in atmospheric particulate matter.

## Materials and methods

### Sampling site

Resuspended particles samples and one RD sample were collected on the road side of SS11 which connects Venice to the mainland. The sampling site (45°28′27.10″N; 12°15′10.26″E) is near a streetlamp of southern roadway (toward Venice), located before two crossroads leading to the northeastern areas of industrial port and to the nearby public park “San Giuliano”, as shown in Fig. 1. SS11 is among the busiest roads of the Venice mainland; indeed, the nearest vehicular traffic monitoring station, which is located about 2.5 km toward Venice from the sampling site, detected about 33,000 vehicles per day in 2012. About 75% of the fleet composition is characterized by vehicles shorter than 5 m, 15% longer than 7.5 m and 10% between 7.5 and 5 m long (Valotto et al. 2015). Finally, according to the authors’ experience, the traffic flow at the sampling site is faster than the respective speed limit of 70 km h<sup>-1</sup>.

The resuspended particles sample is composed of an 8×30×0.125 mm double-sided conductive carbon tape typically used for SEM analysis pasted onto a 20×50×1 mm aluminum foil. Samples were fixed to a street lamp on the road side, about 50 cm from the road edge strip, from December 19, 2016, to January 9, 2017. Heights and



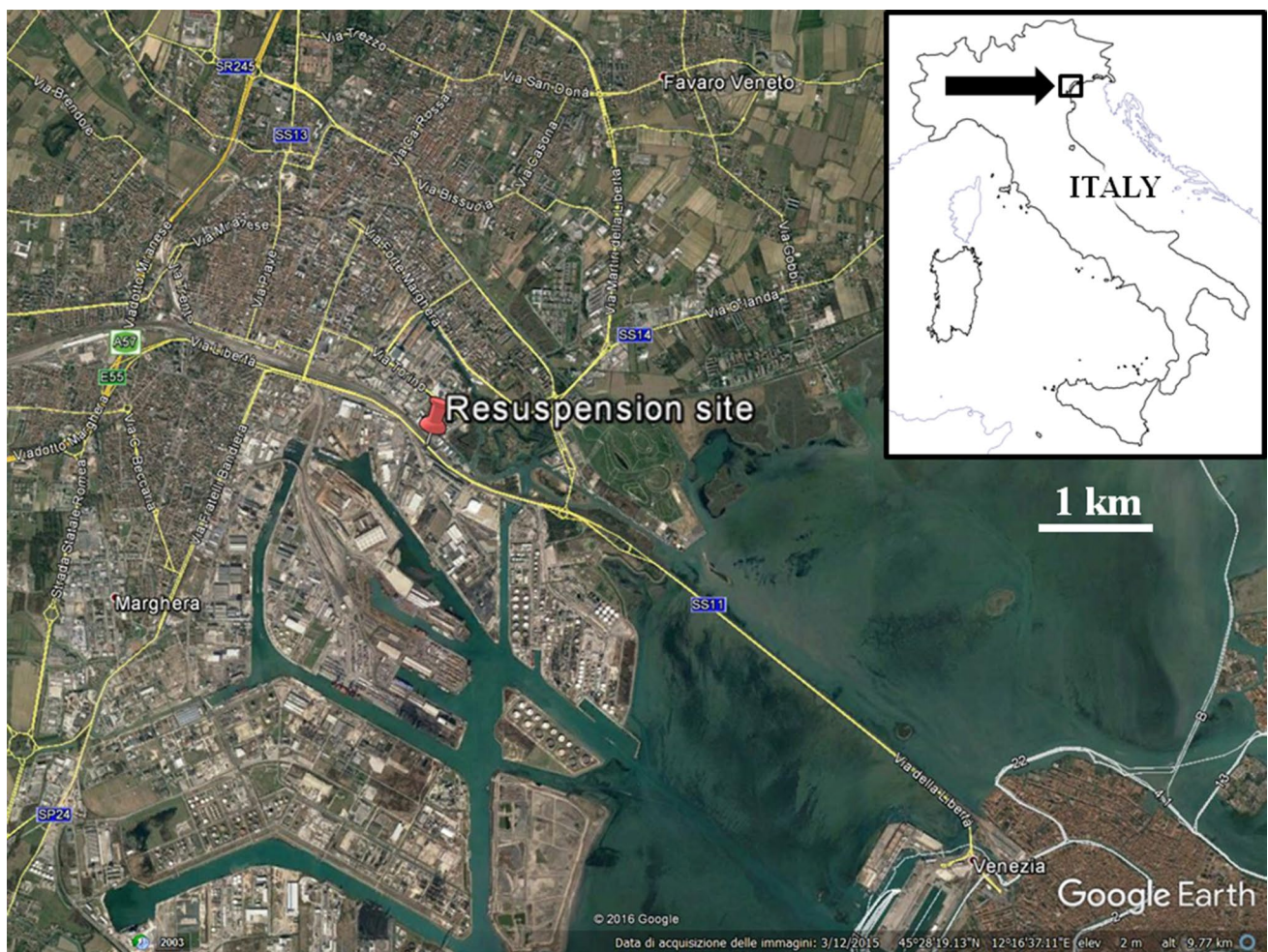


Fig. 1 Sampling site

**Table 1** Heights and exposure durations of resuspended particles samples

Sample	Exposure	Recovery	Duration (days)	Height from the road surface (cm)
1L	December 19, 2016	December 20, 2016	1	20
1M		December 20, 2016	1	120
1H		December 20, 2016	1	200
2L	December 21, 2016	December 21, 2016	2	20
2M		December 21, 2016	2	120
2H		December 21, 2016	2	200
4L	December 23, 2016	December 23, 2016	4	20
4M		December 23, 2016	4	120
4H		December 23, 2016	4	200
17bk	December 23, 2016	January 09, 2017	17	200
17L				20
17M				120
17H				200

durations of samplings are reported in Table 1. Samples are labeled combining the respective sampling duration (number of days) and the height of exposition (high, medium, low). Another sample (17bk) was fixed to a pole located about 10 m from the road, on the opposite road side to evaluate contributions different from the vehicular traffic resuspension. Sampling campaign starts after 22 days with no precipitation and was characterized by no rainfall events during the sampling period. The average temperature and wind speed during the campaign were 3.4 °C and 1.2 m s<sup>-1</sup>, respectively. However, wind speed at sampling site was strongly affected by the traffic flow which promoted high turbulence. Resuspended particles samples were characterized with SEM–EDX technique described below.

At the end of the resuspension sampling campaign (January 9, 2017), about 1 kg of RD was collected on the road surface near the streetlamp at issue, using a small broom and a dustpan. Powder was initially dry sieved with a 500- $\mu$ m ASTM standard sieve to eliminate coarser particles and conditioned in an oven at 50 °C for about 4 days. About 50 g of subsample with particle sizes lower than 500  $\mu$ m (RD<sub><500</sub>) was set apart to characterize the respective particle size distribution. A stack of four decreasing sieves (250  $\mu$ m, 125  $\mu$ m, 63  $\mu$ m and 37  $\mu$ m) was used to separate (dry sieving) the remaining part of the sample. Sieved fractions of the sample were stored in PTFE bottles until analysis. To identify correlations among chemical compositions and particle sizes, different amounts of subsamples with particle size lower than 37  $\mu$ m (RD<sub><37</sub>) and between 37 and 63  $\mu$ m (RD<sub>37–63</sub>) (labeled A–L) were mixed as given in Table S1 of supplementary materials and characterized with laser diffraction analysis, ICP-OES and ICP-MS techniques described below.

### SEM–EDX analysis of resuspended particles samples

Resuspended particles were analyzed with SEM–EDX (FEI Quanta 200 FEG ESEM). The instrument is equipped with a field emission gun that operates under high vacuum conditions using the backscattered electron detector at 25 kV. For particle analysis, the working distance and the magnification were set to 10 mm and 150 $\times$ , respectively. The automated particle analysis utility (APA) of Genesis Particle Analysis software (EDAX Inc) (Anderhalt and Swenson 2006) was used to automatically probe particles. Each SEM image is divided into a number of frames that are sequentially scanned for particles, and for each particle, an EDX spectrum is acquired. The minimum particle size chosen

for the analysis and the area selected affect the number of frames. APA returns several morphometric parameters (e.g., shape, diameter and area) and the elemental composition of each particle. The software estimates the particle area by summing all the pixels within the particle. The average diameter of a particle is defined as the diameter of a circle with the same area. The shape (roundness) parameter for a particle is estimated as  $0.08 \times \text{perimeter}^2 \text{ area}^{-1}$ . The shape value of a round particle is 1; the longer the particle, the greater the value of the shape. In this work, the software recognized the features with average diameters larger than 1.5  $\mu$ m as particles. For the chemical characterization, the particle collection time was 150 s. Carbon and oxygen were not included in the quantitative analysis to avoid the contribution from the supporting tape film. Particles giving low X-ray counts were not included in the analysis. All the concentration values (Al, Ca, Cl, Cr, Cu, Fe, K, Mg, Mn, Na, P, S, Si, Ti, Zn) are reported as weight percentage by default. To characterize a statistically representative number of particles, five random areas (1040  $\times$  1200  $\mu$ m<sup>2</sup>) of each sample listed in Table 1 were analyzed to study the particle size characteristics; instead, the respective chemical composition was studied only for particles belonging to four samples exposed for 17 days. Overall, the chemical composition and the morphology of 3470 and 6768 particles were characterized, respectively.

### Particle sizes of RD samples

About 0.5 g of finer subsamples (RD<sub>37–63</sub>, A–L, RD<sub><37</sub>) and about 1.5 g of the RD<sub><500</sub> were separately dispersed in 700 ml of diluted Tween<sup>®</sup>20 (vol/vol = 1/100,000). The size distributions of particles were investigated with a Mastersizer 3000<sup>®</sup> (Malvern, UK) laser particle size analyzer. During measurements, ultrasonication intensity and stirrer speed were set to 50% and 2200 rpm to prevent the aggregation and the sedimentation of suspended particles, respectively. Ten measurements were taken for each powder sample using the Fraunhofer approximation and general purpose analysis model, obtaining very precise results. Subsequently, representative average volume distribution curves were calculated processing only measurements with weighted residual lower than 2% (at least eight measurements for each sample).

### ICP-OES and ICP-MS analysis of RD samples

About 75 mg of each fine subsamples (RD<sub>37–63</sub>, A–L, RD<sub><37</sub>) was weighted (0.01 mg resolution) and dissolved

with a microwave-assisted acid digestion method (Ethos 1600, Microwave Labstation Milestone with the following sequence: 5' 250 W, 5' 400 W, 5' 600 W, 60' 0 W, 5' 250 W, 5' 400 W, 5' 600 W, 120' 0 W) using 6 ml of  $\text{HNO}_3$ , 2 ml of  $\text{H}_2\text{O}_2$  and 1 ml of HF of analytical grade. Liquid samples were allowed to cool for 2 h, and 1 ml of  $\text{H}_3\text{BO}_3$ -saturated solution was added to contrast the effect of HF. Afterward, the resulting solution was filtered on PTFE filters ( $0.45 \mu\text{m}$ ) and diluted with water (Milli-Q®) into a 25-ml flask. All digested samples were then stored in Teflon bottles until analysis performed with ICP-OES (Perkin Elmer 5300DV) and ICP-MS (PerkinElmer NexION 350X). ICP-OES and ICP-MS are well-established techniques for particulate matter analysis. However, using ICP-MS instead of ICP-OES is mandatory to characterize trace metals with concentration lower than  $1 \mu\text{g kg}^{-1}$  (1 ppb). In this work, elements Al, Ba, Ca, Cr, Cu, Fe, K, Mg, Mn, Na, Ni, Pb, S, Ti and Zn were detected with ICP-OES, while Ag, As, Cd, Co, Li, Mo, Sb, U and V were analyzed with ICP-MS. Further quality control details are reported in supplementary materials (S2).

### Statistical analysis

Correlation coefficients and cluster analysis (CA) were used to study relations between resuspended particles and RD particles.

As regards the resuspended particles samples, all particles (6768) were included for studying the size distributions. Instead, after a first check of about 500 EDX spectra characterized by low CPS values, 76 particles characterized by a low signal-to-noise ratio were excluded from the dataset. SEM–EDX data of samples exposed for 17 days were merged in a single dataset (composed of 3394 particles and 17 variables, i.e., shape, diameter and elemental concentrations) and examined with CA. According to Becherini et al. (2017), data were normalized by maximum value to make the intensity ranges of all variables comparable. Ward's method and squared Euclidean distance were used to identify the main groups of particles.

As regards the finer RD samples ( $\text{RD}_{37-63}$ , A–L,  $\text{RD}_{<37}$ ), to reduce the number of variables related to the particle size distributions, the respective dataset was compacted by adding the percentage volumes of particles belonging to size groups of  $5 \mu\text{m}$  width.

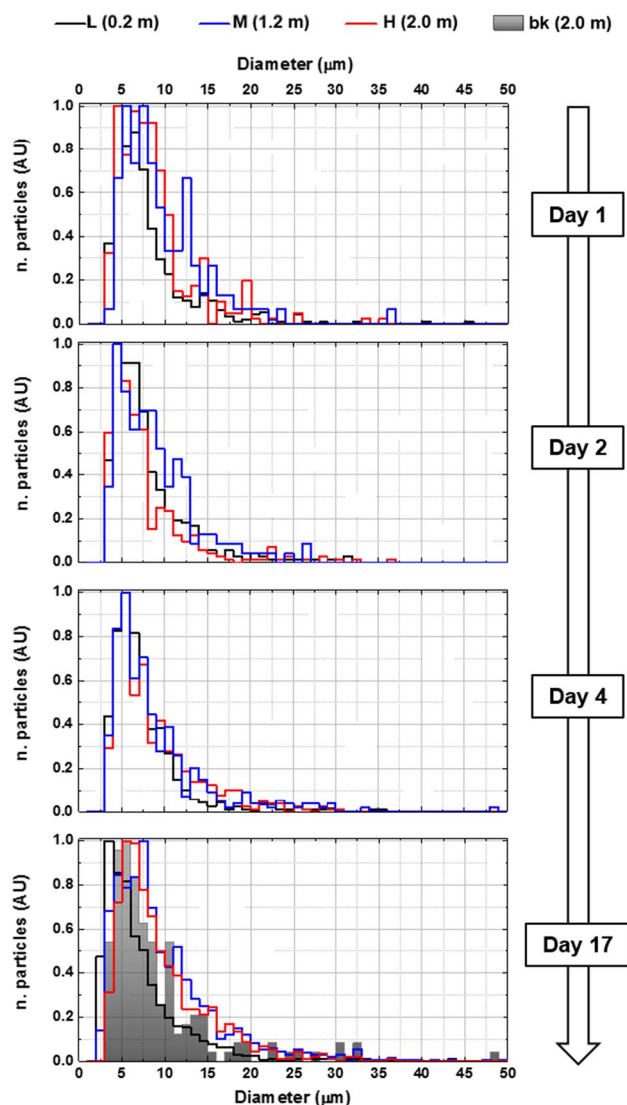


**Fig. 2** Normalized particle size distribution of resuspended particle samples (resolution:  $1 \mu\text{m}$ ). Plots are grouped by the same sampling duration; the arrow gives the time sequence

## Results and discussion

### Resuspended particles samples

The panels of Fig. 2 show the normalized particle size distributions of resuspended particle samples, while Table 2 shows some related statistics.

Results show that: (1) the majority of particles are smaller than  $10 \mu\text{m}$ ; (2) the number of collected particles increases



**Table 2** Statistics related to the size distribution of resuspended particle samples

Sample	Particles collected (n°)	Covered area (%)	Diameter ( $\mu\text{m}$ )					
			Average	Median	Minimum	Maximum	25th percentile	75th percentile
1H	111	0.14	8.6	7.2	2.9	35.4	5.1	11.1
1M	297	0.30	7.7	6.7	2.9	34.8	4.6	9
1L	519	0.49	7.1	5.6	2.9	44.9	4.1	8.1
2H	156	0.17	8	7	2.9	25.7	4.5	10.2
2M	366	0.31	6.7	5.1	2.9	35.6	3.6	7.7
2L	428	0.35	6.9	5.6	2.9	30.7	4.1	8.2
4H	322	0.40	8.1	6.3	2.9	47.2	4.4	9.7
4M	454	0.53	8	6.3	2.9	52.9	4.4	10
4L	645	0.52	6.7	5.5	2.9	34.8	4.1	7.9
17bk	160	0.22	8.1	5.9	2.9	47.5	4.1	9.5
17H	685	0.96	8.7	7.1	2.9	58.7	4.6	10.7
17M	1172	1.89	9.1	7.1	1.5	56.2	4.6	11.2
17L	1453	1.14	6.2	4.8	1.5	42.6	3	7.6

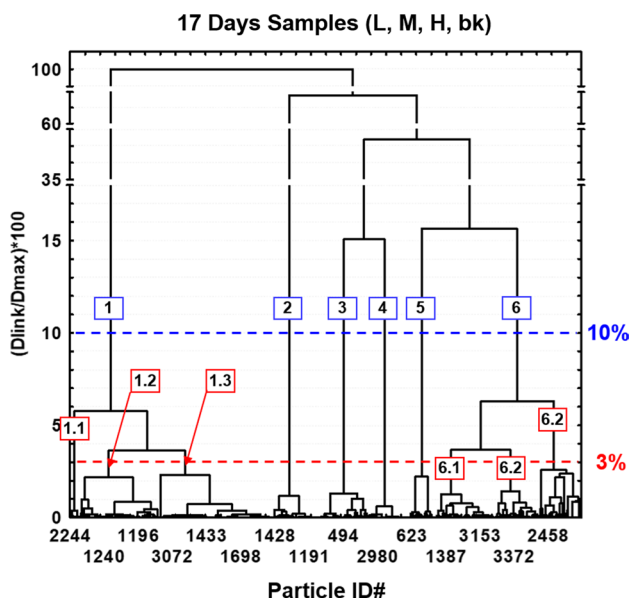


**Fig. 3** Hierarchical tree plot of particles belonging to samples exposed for 17 days. Ward's method and squared Euclidean distance were used as the agglomerative clustering procedure and the metric, respectively. Cluster identification numbers at 3% and 10% levels (horizontal dashed lines) are reported in red and blue, respectively

for samples near the ground; (3) the number of collected particles increases not linearly with the exposition time, probably due to the adhesive efficiency decrease during the sampling campaign; (4) on average samples collected at ground level (xL) show finer particle size distributions; (5) the pattern of the covered area is not completely compatible

with that of the number of particles due to the different particle size distributions; (6) blank sample is characterized by fewer particles and a finer particle size distribution than the sample collected at the same height (17bk vs. 17H).

Figure 3 shows the hierarchical tree plots of 3394 particles performed by clustering only samples exposed for 17 days. Six clusters of particles can be defined setting a threshold of 10% distance, while at 3% distance, the particles can be grouped into ten clusters because the clusters 1 and 6 are divided into three sub-clusters each.

Some statistics related to the variables of each cluster are presented in the box plots of Fig. 4 together with the SEM images of representative particles identified by probing the sample 17M.

The number of particles and the respective average diameter [in brackets] of clusters versus samples are presented in Table 3, while the respective percentage values are reported in Tables S3 and S4 of supplementary materials.

Results show that: (1) each cluster is characterized by a specific chemical composition, highlighting that it is worth performing the analysis with this resolution degree; (2) samples collected close to the road surface show compatible percentage number of particles per cluster but different to that of blank sample (see Table S4), suggesting that near the road the main source of particles is the traffic resuspension; (3) with the exception of clusters 6.1 and 6.3, the number of particles of each cluster decreases with the height of sample exposition further supporting the hypothesis that the main source of these particles is the traffic resuspension; (4); samples collected at ground level (xL) show finer particle size distributions for all cluster



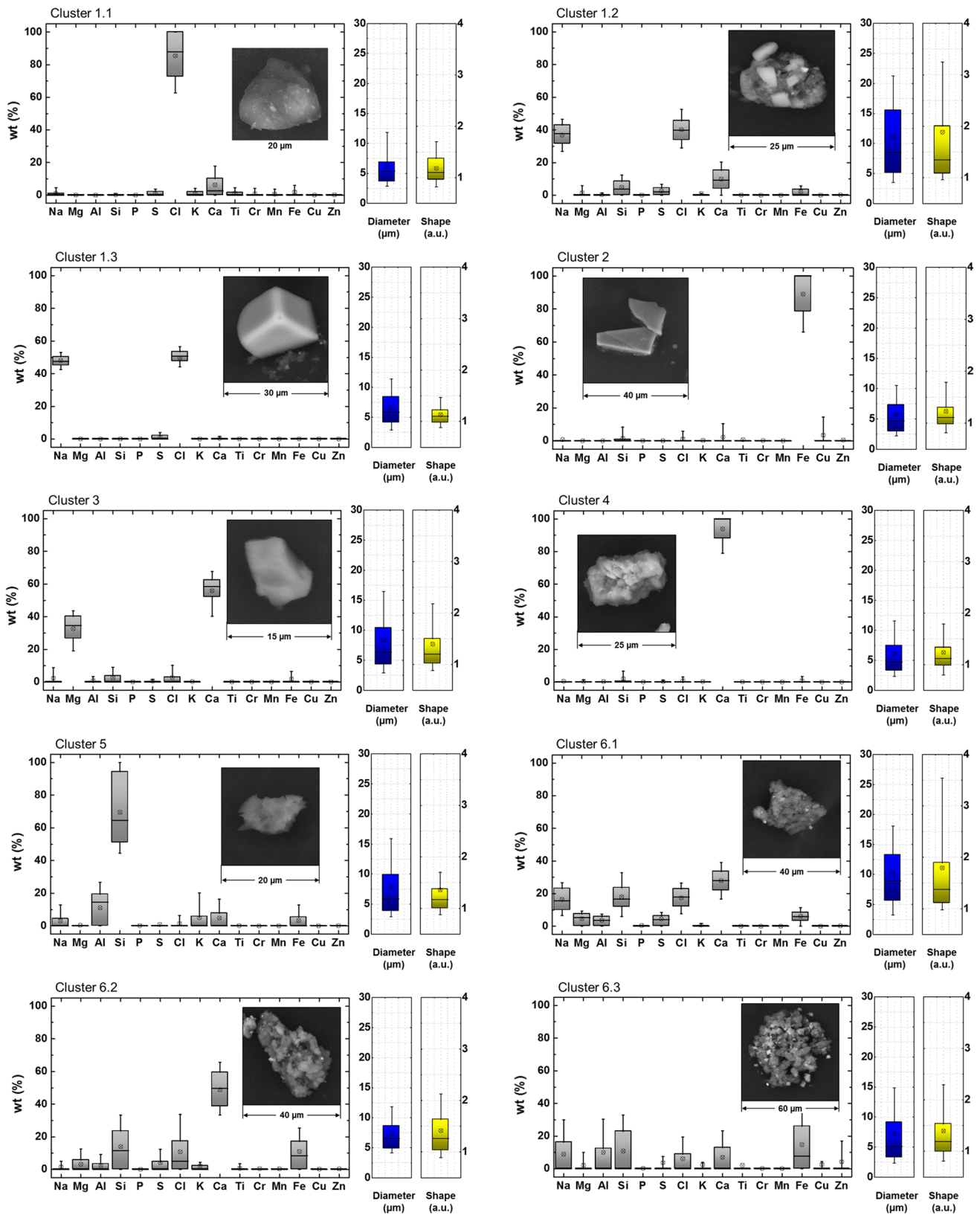


**Fig. 4** Mean (crossed circles), median, 25th and 75th percentiles (boxes), 10th and 90th percentiles (whiskers) values of chemical and morphological variables of particles belonging to each identified cluster. A SEM image of representative particles for each cluster is also reported

**Table 3** Number of particles per sample versus the identified ten clusters; the average diameters are in brackets

Cluster	17bk (n°) [μm]	17H (n°) [μm]	17M (n°) [μm]	17L (n°) (μm)	Total sum (n°) [μm]
1.1	1 [12.5]	4 [7.3]	29 [7.3]	32 [4.9]	66 [6.2]
1.2	8 [10.2]	109 [12.0]	200 [13.4]	208 [8.6]	525 [11.1]
1.3	16 [6.3]	178 [6.8]	242 [7.8]	329 [5.6]	765 [6.6]
2	17 [5.7]	41 [7.5]	83 [6.4]	157 [4.9]	298 [5.7]
3	22 [12.7]	72 [8.6]	97 [9.4]	137 [6.8]	328 [8.3]
4	29 [6.5]	42 [5.8]	69 [8.0]	131 [5.0]	271 [6.1]
5	17 [8.4]	46 [9.2]	56 [9.0]	59 [5.7]	178 [7.9]
6.1	9 [13.9]	91 [11.4]	157 [10.4]	135 [9.1]	392 [10.3]
6.2	14 [7.4]	56 [7.1]	100 [7.4]	125 [5.2]	295 [6.4]
6.3	24 [6.7]	46 [9.2]	120 [7.5]	86 [5.8]	276 [7.2]
Total sum (n°)	157 [8.2]	685 [8.7]	1153 [9.1]	1399 [6.3]	3394 [7.9]

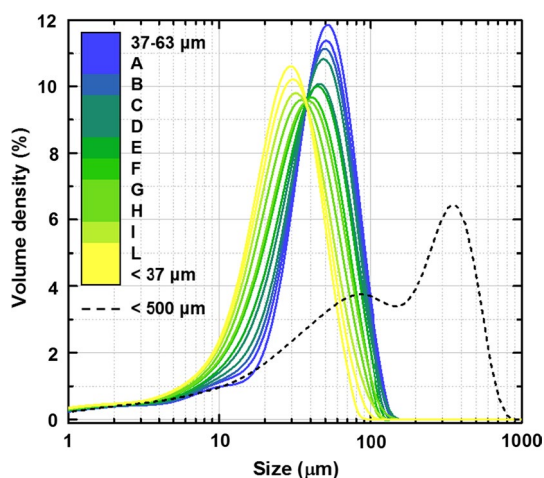


**Fig. 5** Particle size distribution curves of A–L, RD<sub><37</sub>, RD<sub>37–63</sub> and RD<sub><500</sub> subsamples

(see Fig. 2 and Table 2); (5) the cluster 1 is composed of the two most numerous sub-clusters (1.3 followed by 1.2) and the less numerous one (1.1).

To improve the readability of this work, the clusters characteristics are introduced and discussed in “Attribution of sources to identified clusters” section, identifying the main potential source of particles.

## RD samples

Particle size distributions of A–L, RD<sub><37</sub>, RD<sub>37–63</sub> and RD<sub><500</sub> subsamples are reported in Fig. 5. The seeming incongruence between the particle size distributions and the ASTM standard sieves used to create the subsamples are related to the presence of: (1) particles with elongated shape crossing the mesh of sieves which are revealed larger than

their lower diameter and (2) groups of several fine particles which are not disaggregated during the dry sifting (Valotto et al. 2018).

The mode of RD<sub><500</sub> is 354 μm, while the percentage volume of particles lower than 1 μm, 2.5 μm and 10 μm is, respectively, 0.7%, 2.8% and 8.7%. These results confirm that resuspended RD could be an important source of particulate matter. RD<sub><37</sub> and RD<sub>37–63</sub> show significantly different curves, while A–L subsamples are characterized by intermediate and progressive volume contributions according to the respective mass contributions of Table S1 of supplementary materials.

Elemental concentrations of RD<sub><37</sub> and RD<sub>37–63</sub> subsamples and respective uncertainties are reported in Table 4. The rightmost columns of Table 4 show only the significant ( $p < 0.05$ ) Pearson correlation coefficients between element concentrations and particle sizes. Specifically, for each element just the average values of particle sizes lower than 35 μm and higher than 40 μm are reported because the respective values are quite uniform as proved by the standard deviation values in parenthesis.

The significant correlation coefficients between elements are given in Table S5 of supplementary materials.

Elements with a crustal origin such as Ca, Fe, Mg, Na and K give a high mass contribution to both fractions of RD samples (about 15%). Ba, Sb and U are significantly more concentrated in particles smaller than 35 μm, followed by Mo and Mn and to a lesser extent by V and S.

## Attribution of sources to identified clusters

The sub-cluster 1.1 is characterized by high concentration of Cl and moderate concentration of Ca. These particles show round appearance (shape = 1.2), an average diameter of about 6 μm, and constitute the less numerous group. Particles



**Table 4** Element concentrations of RD<sub><37</sub> and RD<sub>37–63</sub> subsamples and significant (*p* value < 0.05) correlation values between element concentrations and particle sizes

Element	RD <sub>&lt;37</sub> ( $\delta$ )	RD <sub>37–63</sub> ( $\delta$ )	Correlation values with particle sizes < 35 $\mu\text{m}$ (SD)	Correlation values with particle sizes > 40 $\mu\text{m}$ (SD)
Ca (%)	10.2 (0.1)	10.3 (0.1)		
Fe (%)	1.71 (0.01)	1.75 (0.02)		
Mg (%)	1.33 (0.01)	1.56 (0.02)		
Na (mg g <sup>-1</sup> )	8.1 (0.1)	7.7 (0.1)		
K (mg g <sup>-1</sup> )	6.7 (0.1)	6.5 (0.1)		
S (mg g <sup>-1</sup> )	3.8 (0.2)	3.6 (0.4)	0.61 (0.01)	-0.62 (0.02)
Ti (mg g <sup>-1</sup> )	3.50 (0.04)	3.57 (0.04)		
Zn (mg g <sup>-1</sup> )	1.54 (0.01)	1.42 (0.01)		
Cu (mg g <sup>-1</sup> )	1.22 (0.01)	1.13 (0.01)		
Mn (mg g <sup>-1</sup> )	1.09 (0.01)	1.02 (0.01)	0.81 (0.01)	-0.81 (0.01)
Cr ( $\mu\text{g g}^{-1}$ )	571 (6)	563 (5)		
Ba ( $\mu\text{g g}^{-1}$ )	485 (3)	407 (4)	0.97 (0.01)	-0.971 (0.003)
Al ( $\mu\text{g g}^{-1}$ )	304 (7)	250 (7)		
Pb ( $\mu\text{g g}^{-1}$ )	144 (4)	152 (4)		
Sb ( $\mu\text{g g}^{-1}$ )	83 (6)	59 (4)	0.96 (0.01)	-0.956 (0.004)
Ni ( $\mu\text{g g}^{-1}$ )	71.5 (0.5)	65.2 (0.9)		
V ( $\mu\text{g g}^{-1}$ )	61.3 (0.4)	53.1 (0.5)	0.624 (0.003)	-0.62 (0.01)
Mo ( $\mu\text{g g}^{-1}$ )	28.4 (0.3)	21.4 (0.2)	0.812 (0.003)	-0.811 (0.004)
Li ( $\mu\text{g g}^{-1}$ )	14.2 (0.1)	13.4 (0.2)		
Co ( $\mu\text{g g}^{-1}$ )	8.63 (0.09)	7.9 (0.1)		
As ( $\mu\text{g g}^{-1}$ )	4.31 (0.02)	3.57 (0.03)		
Cd ( $\mu\text{g g}^{-1}$ )	2.4 (0.2)	3.2 (0.2)		
U ( $\mu\text{g g}^{-1}$ )	1.64 (0.05)	1.38 (0.04)	0.916 (0.005)	-0.919 (0.005)
Ag ( $\mu\text{g g}^{-1}$ )	1.3 (0.1)	1.2 (0.1)		

Concentration uncertainties and standard deviations of correlation coefficients are in parenthesis

belonging to sub-cluster 1.1 are exclusively detected in the samples collected near the ground (17L and 17M). According to the Italian national road safety authority (ANAS 2017), the shedding of anti-ice material is the most likely source of these particles. Anti-ice material is composed of limestone or river sand ( $\approx 50\%$ ) properly mixed with calcium chloride ( $\approx 5\text{--}10\%$ ) and sodium chloride ( $\approx 40\text{--}45\%$ ). The high purity of these particles (the concentrations of other probed elements are close to zero) is likely due to the high solubility of CaCl<sub>2</sub> in the water (740 g l<sup>-1</sup> at 293 K) that originates from the ice melting during the warm hours of the day, the subsequently traffic resuspension of drops which impact on the sample, and the consecutive recrystallization of the salt at issue due to the water evaporation. CaCl<sub>2</sub> is also often used as a dust suppressant in northern and central Europe (AIRUSE LIFE 11 ENV/ES/584 2016). However, since ANAS does not use this type of salt to limit the resuspension and samples collection occurred during winter, we are confident that it was used to limit the asphalt freezing.

Sub-cluster 1.2 is the second numerous group characterized by the presence of Na and Cl and to a less extent of Si, S, Ca and Fe. Particles belonging to this group are characterized by an elongated shape (shape = 1.9) and an average diameter of about 11  $\mu\text{m}$  (the greatest value). Particles look like conglomerates of different materials. Precisely, the representative particle image of Fig. 4 shows noticeable cubic crystals of halite, suggesting the presence of Na and Cl and traces of Ca, Si, Fe, Mg and Al, which are typical constituents of local soil particles (Valotto et al. 2018). The likely source of these particles is the shedding of anti-ice material, according to the above consideration for cluster 1.1. Indeed, in this matrix the sodium chloride is already mixed with limestone or river sand which is composed of the above-mentioned trace elements. Moreover, another aggregation mechanism between the sodium chloride and the local soil particles previously deposited on the asphalt could be the cyclic process of solubilization–crystallization promoted by the moisture variation of the road surface during the day.

Sub-cluster 1.3 is the most numerous group. It is characterized mostly by Na and Cl. (Traces of S are visible.) Particles are nearly round (shape = 1.1) and characterized by an average diameter of about 7  $\mu\text{m}$  (slightly lower than those of cluster 1.2). As shown in Fig. 4, particles look like cubic crystals, typical of halite. As in the case of cluster 1.1, the high purity of these particles could be related to the high solubility of NaCl (358  $\text{g l}^{-1}$  at 293 K) and the subsequently drops resuspension. However, due to the proximity of the Venice lagoon and the sea, the sea spray contribution cannot be ruled out (Valotto et al. 2018).

On average, cluster 1 particles were also detected in Becherini et al. (2017) but with a lower resolution level. Specifically, NaCl-rich particles were detected on coated marble samples exposed outdoors for a year in Florence (Italy). However, the percentage number of these particles in Becherini et al. (2017) was significantly lower than in this study. This difference is likely due to the sampling characteristics (sampling height, sampling duration) and in particular to the distance between the road and the sea.

Cluster 2 particles show high concentrations of Fe, an average diameter of about 6  $\mu\text{m}$  (the smallest value) and a round appearance (shape = 1.2). The concentration of soil tracers is close to zero; hence, we hypothesize that these particles are not related to the Fe-rich minerals contained therein, but have an anthropogenic origin. Indeed, as shown in Fig. 4 the representative particles look like splinters characterized by sharp edges and irregular shape probably related to abrasion process, such as deriving from brake pads and disks friction. Precisely, the latter are made of steel which is mainly composed of Fe and C. It is worth reminding that elements C and O were not included in the EDX quantitative analysis, in order to avoid the adhesive tape contribution; due to this, the presence of steel scraps or of the different oxides and hydroxides forms cannot be suitably investigated. In this view, we identify as generic source of these particles the wear process of vehicular parts iron rich. Compared with other groups, the particles of this cluster are in percentage more concentrated in the sample collected at ground level (see 17L in Table S3) likely due to their high density, which results in a lower range of debris directly emitted and in a lower resuspension yield of deposited particles. Indeed, unlike the particles of cluster 1 which mainly originate from the resuspension process as mentioned above, in this case it is not possible to distinguish between particles sourced to abrasion process directly and to resuspended particles. It should be noted that such iron-rich particles were associated with traffic non-exhaust sources and with RD resuspension in precedent studies (Becherini et al. 2017).

Cluster 3 particles are characterized by an average diameter of about 8  $\mu\text{m}$ , a slightly elongated appearance (shape = 1.4) and high concentrations of Ca and Mg, compatible with the mineral Dolomite. Limestone and dolostone are the main constituents of sediments and gravels of the study area, since the study area catchment basin is mainly composed of carbonate rocks (Fontana et al. 2008). Indeed, the representative image of Fig. 4 shows an evident rhombohedral morphology, typical of dolomite mineral.

Cluster 4 particles show the typical crystalline morphology of calcite (trigonal system), compatible with the high concentration of Ca. These particles are characterized by a round appearance (shape = 1.2) and an average diameter smaller than those of cluster 3 (about 6  $\mu\text{m}$ ), which is in accordance with the lower hardness of this mineral. Cluster 4 particles are more concentrated in the blank sample (see 17bk in Table S3), suggesting the influence of other sources besides the road traffic in the study area.

Particles of cluster 5 have a slightly elongated appearance (shape = 1.4) and are characterized by an average diameter of about 8  $\mu\text{m}$ . The high concentrations of Si and moderate values of Al are ascribable to the presence of aluminosilicate minerals. Indeed, the representative image of Fig. 4 shows the characteristic layered structure of clay minerals. As for the case of cluster 4 particles, also cluster 5 particles are in percentage more concentrated in the blank sample and in the sample collected at high height (see 17bk and 17H in Table S3), suggesting that in the monitoring area there are other sources besides the road traffic.

As stated in the characterization of cluster 1, a significant source of particles belonging to clusters 3, 4 and 5 is the shedding of anti-ice material which is composed of limestone or river sand ( $\approx 50\%$ ). Indeed, according to Pezzolo et al. (2017) who have characterized the sand composition of three rivers close to the sampling site at issue, this matrix is composed of a significant fraction of carbonate and silicates. Moreover, another source of particles belonging to clusters 3 and 4 could be the wear of the road surface which is composed of bitumen and a mineral mixture. Carbonate rocks such as limestone and dolostone are commonly mixed with bitumen in this regard (Zannoni et al. 2016). Furthermore, another source of particles belonging to cluster 4 and 5 could be the resuspension of the finer fractions of the ballast of the close railways and of the gravel used to cover the path of a garden near the sampling sites. Finally, although the carbonate and silicate minerals are also soil constituents, we are inclined to exclude the resuspension of this matrix from the list of the representative sources of the clusters 3–5 due



**Table 5** Mass of particles for each sample versus the identified ten clusters

Cluster	17bk (ng mm <sup>-2</sup> )	17H (ng mm <sup>-2</sup> )	17M (ng mm <sup>-2</sup> )	17L (ng mm <sup>-2</sup> )	Total sum (ng mm <sup>-2</sup> )
1.1	0.4	0.3	5.4	1.4	7.5
1.2	3.5	108.5	274.5	92.5	478.9
1.3	0.9	18.0	37.4	21.0	77.4
2	2.4–3.7	24.5–37.7	15.9–24.5	30.9–47.6	73.8–113.5
3	26.7	22.4	66.9	44.5	160.5
4	9.4	2.9	17.1	19.2	48.6
5	7.0–9.3	28.0–37.4	31.3–41.7	10.6–14.1	76.9–102.5
6.1	29.7	57.5	131.0	65.3	283.5
6.2	3.1	7.9	23.9	8.6	43.5
6.3	3.2	38.2	56.7	10.6	108.8
Total sum (ng mm <sup>-2</sup> )	86.3–89.9	308.4–330.9	660.3–679.3	304.5–324.7	1359.4–1424.8

to the high pureness of particles and especially because this source is better explained by the cluster 6.

Precisely, although cluster 6 (the second most numerous) is composed of three sub-clusters characterized by different shapes, average diameter and different concentration ratios of the typical elements with crustal origin such as Al, Ca, Cl, Fe, Mg, Na, S and Si (Valotto et al. 2018), all particles look like conglomerates of different materials as in the case of sub-cluster 1.2. However, in these clusters the concentrations of Na and Cl are significantly lower, suggesting also additional binding materials such as CaCO<sub>3</sub> or CaSO<sub>4</sub> which further suggest the resuspension of soil particles previously deposited on road surface. Indeed, this kind of particles was also detected in Becherini et al. (2017), which were ascribed to the resuspended crustal dust.

Particles of sub-cluster 6.1 are characterized by an average diameter of about 10 µm (the second higher value) and an elongated appearance (shape = 1.8). These show high concentrations of Ca, Cl, Si and Na and traces of Fe, Mg, Al and S. Unlike groups so far described, these particles are more concentrated on sample collected at medium height.

Particles of sub-cluster 6.2 are finer than those of the previous one (about 6 µm) and are characterized by a slightly elongated appearance (shape = 1.4). These show high concentrations of Ca, followed by Si, Fe and Cl.

Finally, particles of sub-cluster 6.3 show an average diameter of about 7 µm, a slightly elongated appearance (shape = 1.4), and, as in the case of sub-cluster 6.1, are more concentrated on sample collected at medium height. These particles are characterized by high concentrations of Fe, Si, Na, Al, Ca, Cl and Zn. We suppose that these resuspended particles are an admixture of vehicular debris and soil particles previously deposited on the road surface because: (1) the high concentrations of iron which is the representative

elements of the cluster 2 (wear of vehicular parts Fe rich and (2), compared with other groups, the highest concentrations of Zn which is a tracer of the tire wear (Pant and Harrison 2013; Valotto et al. 2017).

At this stage, it is worth noting that particles that look like conglomerate belong to clusters characterized by higher shape values (1.2, 6.1, 6.2 and 6.3) likely because the cohesion process is promoted by the compression of the rolling wheels which confer the typical elongated appearance, in addition to the daily moisture variation of the road surface which induce the solubilization–crystallization of the binder minerals.

### Mass contribution of clustered particles

To conclude, the qualitative mass contributions of identified clusters for each sample were evaluated considering particles size and chemical composition. The following approximations were used to calculate the contributions reported in Table 5:

- All particles were considered spherical, and each volume was calculated using the respective average diameter. This is a cautionary approach because the contribution of flat particle is overestimated.
- Because the densities of CaCl<sub>2</sub> and halite are similar, 2.2 g cm<sup>-3</sup> was used to evaluate the contributions of cluster 1.
- The density of the pure iron (8.0 cm<sup>-3</sup>) and that of the respective lighter and probable oxide (Fe<sub>3</sub>O<sub>4</sub> = 5.2 g cm<sup>-3</sup>) were used to evaluate the highest and the lowest contributions of cluster 2.



- The density of dolomite and calcite ( $2.8 \text{ g cm}^{-3}$  and  $2.7 \text{ g cm}^{-3}$ , respectively) was used for the clusters 3 and 4, respectively.
- Two generic values were used to evaluate the highest and the lowest contributions of silicates ( $3\text{--}4 \text{ g cm}^{-3}$ ) for the cluster 5.
- According to Yu et al. (1993), the generic particle density of mineral soils ( $2.6 \text{ g cm}^{-3}$ ) was used to evaluate the contributions of particles belonging to cluster 6.

Examining Table 5, it is worth noting that:

- As in the case of the number of particles, on average the cluster 1 gives the highest mass contribution; however, the respective sub-cluster characterized by the greater contribution is 1.2 (instead of 1.3) due to its larger particle size.
- As in the case of the number of particles, the second largest mass contribution is provided by cluster 6.
- Despite the highest density value of cluster 2, its mass contribution is moderate due to the respective low particle sizes.
- Although the significant particle number contribution, the lowest mass contribution is provided by cluster 4 due to its low particle size.
- Unlike the particle number contribution, with the exception of clusters 2 and 4, the highest mass contributions were detected on sample collected at medium height (17M) due to the finer particle size distribution of the sample collected at ground level (17L), as depicted in Fig. 2 and Tables 2 and 3. It is worth noting that the total mass contribution of samples 17L and 17H is comparable.

Although the particle sizes of resuspended particle samples are significantly finer than those of the finest RD samples (Figs. 2 vs. 5), the chemical compositions of both matrices are compatible. Indeed, the most concentrated elements in  $\text{RD}_{<37}$  and  $\text{RD}_{37-63}$  are Ca, Fe, Mg and Na, which are the representative elements of clusters providing the highest mass contributions. Due to the coarser particle size of RD samples, a greater soil contribution for Ca, Fe and Mg is plausible. Instead, according to resuspended particles, the most likely source of Na in RD samples is the anti-ice material and to a lesser extent the closeness to the Venice lagoon. About the health concerns related to the traffic resuspension source, 1.2 m is the most critical height as regards the mass contributions, although at ground level the concentration of finest particles, which

deeply penetrate into the respiratory system, is highest. Moreover, although on average analyzed particles elemental composition is seemingly not alarming, the presence of health concern elements such as As, Cd, Ni and Pb, at concentrations lower than the detection limit of SEM–EDX analysis, is not ruled out. Indeed, these elements in addition to Cr, Ba, Al, Sb, V, Mo, Li, Co, U and Ag were detected in  $\text{RD}_{<37}$  and  $\text{RD}_{37-63}$  samples at concentrations lower than  $1 \text{ mg g}^{-1}$  (see Table 4). It is worth noting that most of the above-mentioned elements are more correlated and then concentrated in the finest fractions of RD. In this context, according to Sanders et al. (2003) it is plausible that the finest resuspended particles, in particular those lower than  $1.5 \mu\text{m}$  which were not analyzed, also contain the above-mentioned trace elements.

### Key aspects to explore in future studies

Finally, because this research is a preliminary study which aims at suggesting an alternative way to study the particles related to traffic emissions, it is worth pointing out its critical issues which will have to be explored in the future:

- Because the number of particles which adhere to the tape is not linearly dependent on exposure time, this sampling method is not suitable to evaluate the flux of resuspended particles as in the case of passive aerosol samples used in Orza et al. (2009). In this view, it is desirable to perform other sampling campaign to evaluate the efficiency of different adhesive substrates as a function of exposure time.
- A selective sampling due to the geometrical, mechanical and chemical characteristics of particles (e.g., shape, size, density, momentum, affinity between tape and particle, etc.) could not be ruled out. As mentioned above, it is desirable to perform a dedicated sampling campaign to evaluate the efficiency of others adhesive substrates.
- EDX analysis does not allow discriminating the tape contribution when smaller particles are probed. As mentioned above, the use of other adhesive substrate with different chemical compositions could overcome this issue.
- Particles smaller than the X-ray generation volume for SEM–EDX are not carefully characterized; therefore, the limit of average diameter  $1.5 \mu\text{m}$  was set in this work to recognize analyzable particles. Due to this, the finest particles related to brakes and tires wear (Kwak et al. 2013) were not characterized.
- Because the RD composition is site specific and its resuspension is significantly related to the weather and traffic-



related parameters (Valotto et al. 2015), it is desirable to iterate this sampling campaign with other conditions (e.g., season, traffic flux, road surface, etc.).

## Conclusion

Results confirm that resuspension of road traffic-related particles can contribute significantly to atmospheric particulate matter. In this work, we performed a deep characterization of road dust and resuspended particles larger than 1.5  $\mu\text{m}$ , highlighting the differences as a function of the sampling height from the road surface. Six groups of resuspended particles were identified, mainly related to the shedding of anti-ice material, to the soil resuspension and to road surface and vehicle parts wear. Although the highest number of particles was detected at ground level for almost all groups, the greatest mass contributions were identified at about 1.2 m above the road due to the contribution of coarser particles. Finally, because this research is a preliminary study suggesting an alternative way to study the particles related to traffic emissions, its critical issues were pointed out.

**Acknowledgments** This research received no specific Grant from any funding agency in the public, commercial or not-for-profit sectors.

## References

- AIRUSE LIFE 11 ENV/ES/584 (2016) The efficacy of dust suppressants to control road dust re-suspension in northern and central Europe
- Amato F, Cassee FR, van der Gon HACD, Gehrig R, Gustafsson M, Hafner W, Harrison RM, Jozwicka M, Kelly FJ, Moreno T, Prevot ASH, Schaap M, Sunyer J, Querol X (2014) Urban air quality: the challenge of traffic non-exhaust emissions. *J Hazard Mater* 275:31–36
- Amato F, Zandveld P, Keuken M, Jonkers S, Querol X, Reche C, van der Gon HACD, Schaap M (2016) Improving the modeling of road dust levels for Barcelona at urban scale and street level. *Atmos Environ* 125(Part A):231–242
- ANAS (2017) Direzione Ingegneria e Verifiche, elenco prezzi 2017 MO.2017 – Rev.0 Manutenzione Ordinaria. <http://www.stradanas.it/sites/default/files/pdf/4.5/MO%20-%20LISTINO%20PREZZI%202017%20-%20Manutenzione%20Ordinaria.pdf>. Accessed 20 Nov 2018
- Anderhalt R, Swenson L (2006) Applications for automated particle analysis. *Microsc Today* 14(5):22–26
- Becherini F, Pastorelli G, Valotto G, Gambirasi A, Bianchin S, Favaro M (2017) Effects of protective treatments on particle deposition and colour variation in stone surfaces exposed to an urban environment. *Prog Org Coat* 112:75–85
- Bukowiecki N, Gehrig R, Lienemann P, Hill M, Figi R, Buchmann BFM, Richard A, Mohr C, Weimer SO (2009) PM10 emission factors of abrasion particles from road traffic. *Schweizerische Eidgenossenschaft*
- Denby BR, Sundvor I, Johansson C, Pirjola L, Ketzler M, Norman M, Kupiainen K, Gustafsson M, Blomqvist G, Omstedt G (2013) A coupled road dust and surface moisture model to predict non-exhaust road traffic induced particle emissions (NORTRIP). Part 1: road dust loading and suspension modelling. *Atmos Environ* 77:283–300
- EMEP/EEA (2016) Air pollutant emission inventory guidebook 2016: technical guidance to prepare National Emission Inventories (1.A.3.b.vi –vii Road Tire and Brake Wear 2016). <https://www.eea.europa.eu/publications/emep-eea-guidebook-2016>. Accessed 20 Nov 2018
- Fontana A, Mozzi P, Bondesan A (2008) Alluvial megafans in the Venetian–Friulian Plain (north-eastern Italy): evidence of sedimentary and erosive phases during Late Pleistocene and Holocene. *Quat Int* 189(1):71–90
- Grigoratos T, Martini G (2015) Brake wear particle emissions: a review. *Environ Sci Pollut Res* 22(4):2491–2504
- INventario EMISSIONI Regione Veneto (INEMAR) (2006) Emission inventory of Veneto Region (in italian). <http://www.arpa.veneto.it/temi-ambientali/aria/emissioni-di-inquinanti/inventario-emissioni> Accessed 20 Nov 2018
- Karanasiou A, Amato F, Moreno T, Lumbreras J, Borge R, Linares C, Bolado E, Alastuey A, Querol X (2014) Road dust emission sources and assessment of street washing effect. *Aerosol Air Qual Res* 14(3):734–743
- Kumar P, Pirjola L, Ketzler M, Harrison RM (2013) Nanoparticle emissions from 11 non-vehicle exhaust sources: a review. *Atmos Environ* 67:252–277
- Kwak JH, Kim H, Lee J, Lee S (2013) Characterization of non-exhaust coarse and fine particles from on-road driving and laboratory measurements. *Sci Total Environ* 459:273–282
- Orza JAG, Cabello M, Mateo J (2009) Simple passive methods for the assessment of the directional and vertical distributions of wind-blown particulates. *Advances in studies on desertification, Murcia*
- Pant P, Harrison RM (2013) Estimation of the contribution of road traffic emissions to particulate matter concentrations from field measurements: a review. *Atmos Environ* 77:78–97
- Pezzolo ADL, Valotto G, Quaranta A (2017) Carbonate and silicate abundance indexing in coarse-grained river sediments using diffuse reflection infrared spectroscopy (DRIFTS) and ion-beam-induced luminescence (IBIL) spectroscopies. *Appl Spectrosc* 71(6):1222–1230
- Rexeis M, Hausberger S (2009) Trend of vehicle emission levels until 2020—prognosis based on current vehicle measurements and future emission legislation. *Atmos Environ* 43(31):4689–4698
- Sanders PG, Xu N, Dalka TM, Maricq MM (2003) Airborne brake wear debris: size distributions, composition, and a comparison of dynamometer and vehicle tests. *Environ Sci Technol* 37(18):4060–4069
- Shi G, Chen Z, Bi C, Wang L, Teng J, Li Y, Xu S (2011) A comparative study of health risk of potentially toxic metals in urban and suburban road dust in the most populated city of China. *Atmos Environ* 45(3):764–771
- Timmers VRJH, Achten PAJ (2016) Non-exhaust PM emissions from electric vehicles. *Atmos Environ* 134:10–17



- United States Environmental Protection Agency (USEPA) (1996) Soil screening guidance: technical background document. Second edition
- Valotto G, Squizzato S, Masiol M, Zannoni D, Visin F, Rampazzo G (2014) Elemental characterization, sources and wind dependence of PM<sub>1</sub> near Venice, Italy. *Atmos Res* 143:371–379
- Valotto G, Rampazzo G, Visin F, Gonella F, Cattaruzza E, Glisenti A, Formenton G, Tieppo P (2015) Environmental and traffic-related parameters affecting road dust composition: a multi-technique approach applied to Venice area (Italy). *Atmos Environ* 122:596–608
- Valotto G, Cattaruzza E, Bardelli F (2017) Multi-edge X-ray absorption spectroscopy study of road dust samples from a traffic area of Venice using stoichiometric and environmental references. *Spectrochim Acta A Mol Biomol Spectrosc* 13:971–978
- Valotto G, Zannoni D, Rampazzo G, Visin F, Formenton G, Gasparello A (2018) Characterization and preliminary risk assessment of road dust collected in Venice airport (Italy). *J Geochem Explor* 190:142–153
- Wan D, Zhan C, Yang G, Liu X, Yang J (2016) Preliminary assessment of health risks of potentially toxic elements in settled dust over Beijing urban area. *J Environ Res Public Health* 13(5):491
- Yu C, Cheng JJ, Jones LG, Wang YY, Faillace E, Loureiro C, Chia YP (1993) Data collection handbook to support modeling the impacts of radioactive material in soil, Argonne National Lab., IL (United States). Environmental Assessment and Information Sciences Div
- Zannoni D, Valotto G, Visin F, Rampazzo G (2016) Sources and distribution of tracer elements in road dust: the Venice mainland case of study. *J Geochem Explor* 166:64–72

